IJMMM International Journal of Minerals, Metallurgy and Materials 矿物冶金与材料学报（英文版）

Understanding the superior mechanical properties of Mg–3Al–Zn alloy sheets: Role of multi-type unique textures

Jun Xu, Jun Zhao, Bin Jiang, Wenjun Liu, Hong Yang, Xintao Li, Yuehua Kang, Nan Zhou, Kaihong Zheng, and Fusheng Pan

Cite this article as:
Jun Xu, Jun Zhao, Bin Jiang, Wenjun Liu, Hong Yang, Xintao Li, Yuehua Kang, Nan Zhou, Kaihong Zheng, and Fusheng Pan, Understanding the superior mechanical properties of Mg–3Al–Zn alloy sheets: Role of multi-type unique textures, *Int. J. Miner. Metall. Mater.*, 30(2023), No. 6, pp. 1104-1112. https://doi.org/10.1007/s12613-023-2603-z

View the article online at SpringerLink or IJMMM Webpage.

International Journal of Minerals, Metallurgy and Materials
Volume 30, Number 6, June 2023, Page 1104
https://doi.org/10.1007/s12613-023-2603-z

Understanding the superior mechanical properties of Mg–3Al–Zn alloy sheets: Role of multi-type unique textures

Jun Xu[1),✉], *Jun Zhao*[2)], *Bin Jiang*[3,4),✉], *Wenjun Liu*[5)], *Hong Yang*[3,4)], *Xintao Li*[1)], *Yuehua Kang*[1)], *Nan Zhou*[1)], *Kaihong Zheng*[1)], *and Fusheng Pan*[1,3,4)]

1) Institute of New Materials, Guangdong Academy of Sciences, Guangzhou 510650, China
2) School of Mechanical and Electrical Engineering, Hunan City University, Yiyang 413002, China
3) National Engineering Research Center for Magnesium Alloys, College of Materials Science and Engineering, Chongqing University, Chongqing 400044, China
4) Chongqing Institute for Advanced Light Metals, Chongqing 400030, China
5) College of Materials Science and Engineering, Chongqing University of Technology, Chongqing 400054, China
(Received: 21 September 2022; revised: 6 January 2023; accepted: 19 January 2023)

Abstract: Mg–3Al–1Zn (AZ31) sheets were produced by transverse gradient extrusion (TGE) process. The flow behavior and dynamic recrystallization during extrusion were systematically analyzed. The microstructures, textures, and mechanical behavior of extruded AZ31 sheet were also analyzed and compared with conventional extruded (CE) sheet. The results showed that fine grain structure and multi-type unique textures were formed in TGE sheet because of the generation of extra flow velocity along transverse direction (TD) and flow velocity gradient along extrusion direction (ED) during extrusion. The basal poles gradually deviated away normal direction (ND) from edge to center of the TGE sheet along TD, and the largest inclination angle at center region reached around 65°. Furthermore, the basal poles inclined from ED to TD 40°–63°, except for the center region of TGE sheet. The TGE sheet presented higher ductility and strain hardening exponent (*n*-value), but lower yield strength and Lankford value (*r*-value) in comparison with the CE sheet. Both the basal <*a*> slip and tensile twins were easy to be activated during deformation, and the largest elongation of 41% and the lowest yield strength of 86.5 MPa were obtained for the ED-center sample in the TGE sheet.

Keywords: transverse gradient extrusion; multi-type unique textures; mechanical properties

1. Introduction

Mg alloys have attained increasingly attention in aerospace and automobile industries as the structural alloys due to the low density, high specific strength, and excellent damping performance [1–4]. However, a few slip systems can be activated under ambient temperature because of the hexagonal close packed (hcp) structure, which leads to poor ductility and formability [5–9]. Therefore, widely industrial applicability of Mg alloys is limited [10–12].

According to previous researches, refining the microstructure and modifying the texture can effectively optimize the tensile properties of Mg alloys [13–16] . Severe plastic deformation (SPD) process including multi-directional forging [17] and accumulative roll bonding (ARB) [18] has been dedicated to achieving the goal of grain refining and tensile property enhancement of Mg alloys [19]. Nevertheless, these technologies are hard to be continuous manufactured and cost highly [20]. Hot extrusion is considered as the most important way to fabricate thin Mg alloy sheets [21–22]. Nevertheless, conventional extruded (CE) Mg alloys sheets present intense basal texture. This phenomenon leads to poor plasticity of Mg alloys at room temperature, resulting in their limited applications [23]. At present, there are two primary approaches to control texture during extrusion: (1) adding some alloying elements, especially rare earth (RE) elements [24–29], and (2) designing processing method such as asymmetric extrusion (AE) [30] and asymmetric porthole die extrusion (APE)[14]. Although Mg alloys with RE elements have been shown to reduce the basal texture, their high cost still hinders the commercial application. Changing the mold structure could offer low-cost solutions. AE and APE [31] processes could provide additional shear strain during extrusion to obtain weak or tilted textures of extruded sheets, which contribute to the enhancement of tensile properties. However, these extruded Mg alloy sheets still present a single type of basal texture characteristic, which is very unfavorable for deformation along different directions and limits the improvement of mechanical properties. In order to coordinate the deformation along different directions and greatly improve the tensile properties, it's urgent to explore an extrusion process to obtain the Mg alloy sheet with

✉ Corresponding authors: Jun Xu E-mail: xujun5@126.com; Bin Jiang E-mail: jiangbinrong@cqu.edu.cn

different tilted texture types.

In our previous research, we proposed the transverse gradient extrusion (TGE) process and found that a unique texture tilted from normal direction (ND) to extrusion direction (ED) and elongated along transverse direction (TD) appeared in the center of the extruded sheet, which led to a significant improvement in the formability [32]. However, there was no systematic investigation into the microstructure and texture of extruded sheet along TD, and the tensile mechanical properties have not been studied. Therefore, the present work was concentrated on the effect of microstructures and texture evolutions along TD during TGE process on the final mechanical properties of Mg alloy sheet. It is expected that the extruded sheet presents multi-type unique textures, and provides a new idea for the texture control of extruded sheet, so as to greatly optimize the tensile properties.

2. Experimental

Fig. 1(a) presents the schematic diagram of TGE die. Cylindrical specimens with 60 mm in height and 80 mm in diameter were machined from the as-cast ingot of commercial Mg–2.95Al–0.87Zn (wt%) alloy. The cast billet was homogenized at 400°C for 24 h followed by cooling in air. After preheating at a temperature of 400°C for 1 h, the prepared cylindrical samples were extruded at 400°C by TGE and CE processes. The extrusion ratio and ram speed were 51:1 and 0.35 mm/s, respectively. The obtained sheets had the dimension with 2 mm in thickness and 56 mm in width.

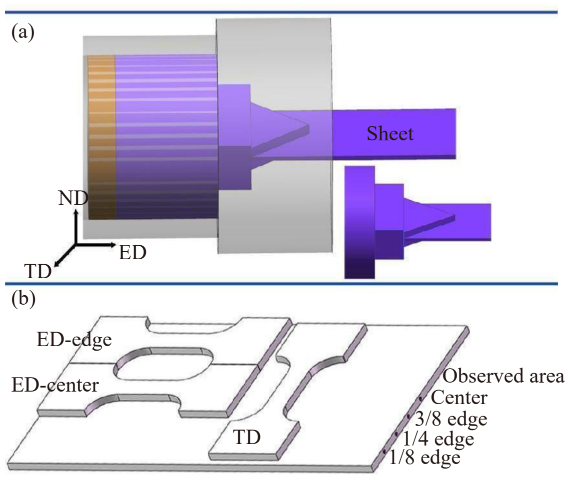

Fig. 1. (a) Schematic diagram of TGE die; (b) sample preparations for tension tests and microstructural observations in the TGE sheet.

Microstructural was examined by electron backscattered diffraction (EBSD) analyses (SEM, JEOL JSM-7800F). The specimens for EBSD analysis were mechanically polished, followed by electro-polishing in an AC2 electrolyte at 20 V for 95 s. All EBSD data were post-processed using the Channel Five software. For the tensile tests, dogbone specimens with 14 mm initial gauge length and 6 mm width were machined from the sheet by cutting along ED and TD. Tensile tests were performed on the CMT6305-300 KN testing machine at a cross-head speed of 2 mm·min^{-1}. Every tensile test was performed three times to guarantee accuracy of experiments. Due to the change of TGE die structure along TD, the microstructure at center, 3/8 edge, 1/4 edge, and 1/8 edge regions of the TGE sheet were examined (termed as TGE-center, TGE-3/8 edge, TGE-1/4 edge, and TGE-1/8 edge regions samples, respectively). The ED tensile specimens of TGE sheet were machined from different positions along TD, entitled as ED-center and ED-edge samples, respectively, as shown in Fig. 1(b).

3. Results

3.1. Microstructure and texture

Fig. 2 shows the inverse pole figure (IPF) maps, pole figures, and the tilting angle distribution of (0002) poles away from ND for CE, TGE-center, TGE-3/8 edge, TGE-1/4 edge, and TGE-1/8 edge regions samples. The CE sheet presents bimodal microstructures containing fine dynamic recrystallized (DRXed) grains and coarse (unDRXed) grains. In contrast, fine and homogeneous microstructure is obtained in the TGE sheet. The average grain sizes of CE, TGE-center, TGE-3/8 edge, TGE-1/4 edge, and TGE-1/8 edge regions samples are approximately 11.8, 6.3, 6.8, 7.3, and 7.8 μm, respectively. The maximum intensities of TGE sheet do not change significantly compared with the CE sheet, while the orientation distributions exhibit evidently different. The CE sheet has typical basal texture with basal poles largely parallel to ND, while the TGE sheet shows different texture characteristics in different regions. The basal texture component completely disappears for the TGE-center region sample, and the elongated basal poles tilt away from ND to ED. Except for the center region, the basal poles of TGE sheet incline away from ED to TD. The basal poles for the TGE-3/8 and TGE-1/4 edge regions samples tilt 40°–63° from ED to TD. The TGE-1/8 edge region sample exhibits basal texture elongating and inclining about 57° away from ED to TD. To the author's knowledge, this multi-type unique textures feature in TGE sheet has not been reported in extruded Mg alloy sheet. The inclinations of (0002) poles away from ND for the TGE-center, TGE-3/8 edge, TGE-1/4 edge, and TGE-1/8 edge regions samples are also analyzed, and they are different from each other. The smallest inclination appeared in the TGE-1/8 region sample ([0002] peak around 25°), while the largest inclination emerged in the TGE-center region sample ([0002] peak around 65°). The inclinations of basal poles away from ND in the TGE sheet gradually decrease from center to edge region.

As mentioned above, the TGE sheet exhibits multi-type unique textures along TD, and these texture characteristics are different from CE sheet. Thus, the microstructure and texture evolutions at center and 1/4 edge regions of extruded sheet during TGE process are investigated. The microstructure evolutions of workpieces at center region before sheet forming during TGE process are presented in Fig. 3. At the

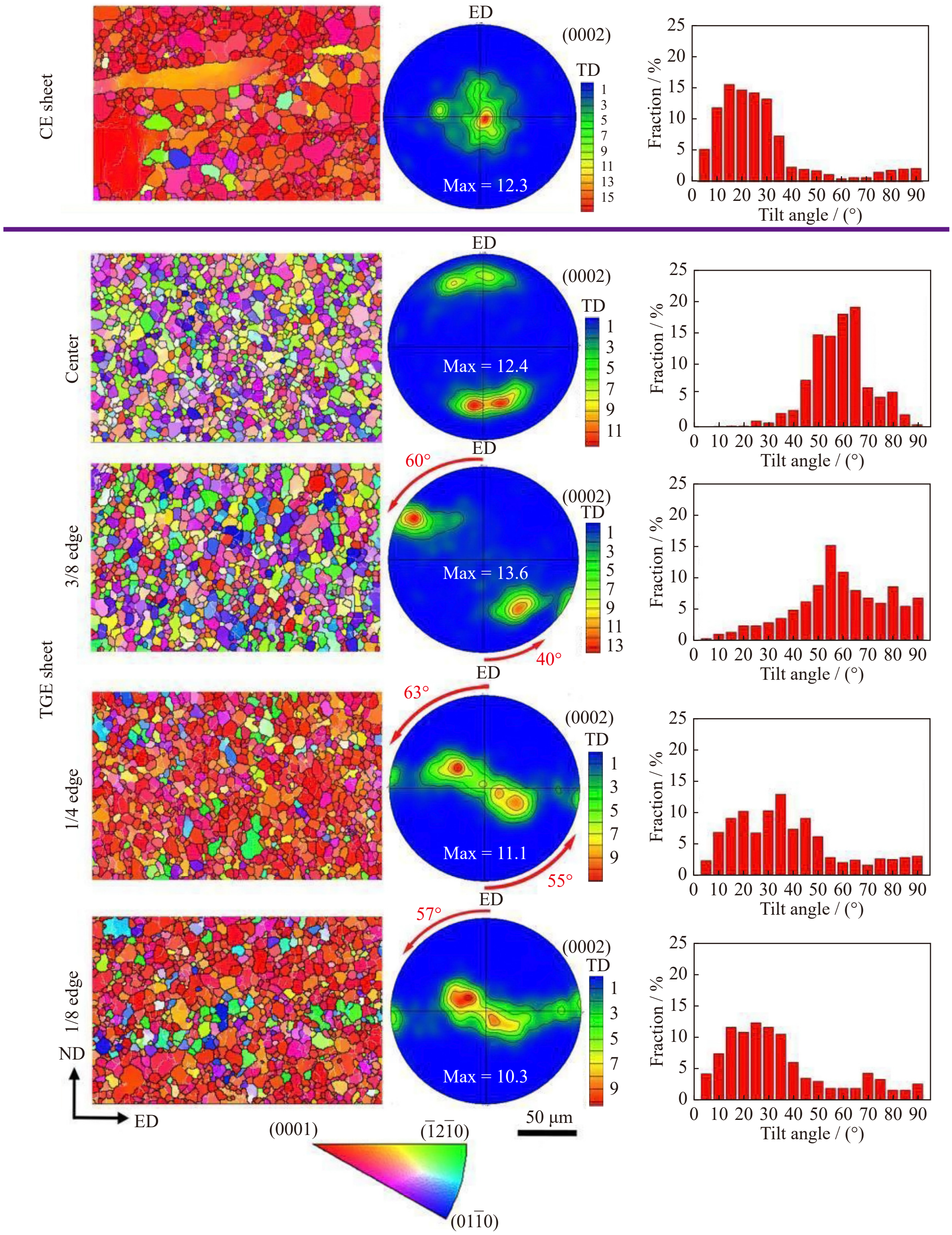

Fig. 2. IPF maps, pole figures, and the tilting angle distribution of (0002) poles away from the ND for CE, TGE-center, TGE-3/8 edge, TGE-1/4 edge, and TGE-1/8 edge regions samples.

early stage of extrusion (at location A), the microstructure is composed of coarse unDRXed and fine DRXed grains. With further deformation, coarse grains gradually change into fine grains due to DRX. At locations C and D, the microstructures are composed of fine uniform DRXed grains. From location A to C, the maximum pole intensities gradually decrease from 16.7 to 8.6 due to the increased DRXed grains. The orientations of unDRXed grains mainly concentrate on the center or adjacent to center in the (0002) pole figures, whereas the DRXed grains distribute randomly [33]. At location B, the sample exhibits TD-tilted texture. Meanwhile, the basal texture components begin to appear. At location C, the basal texture component increases. From location C to D, the maximum pole intensity decreases further because the basal poles are elongated along TD. It is worth noting that this texture characteristic (at location D) is quite different from that of the final extruded TGE sheet.

The microstructure evolutions of workpieces at center region after sheet forming during TGE process are investigated, as shown in Fig. 4. It is obvious that the sample in each

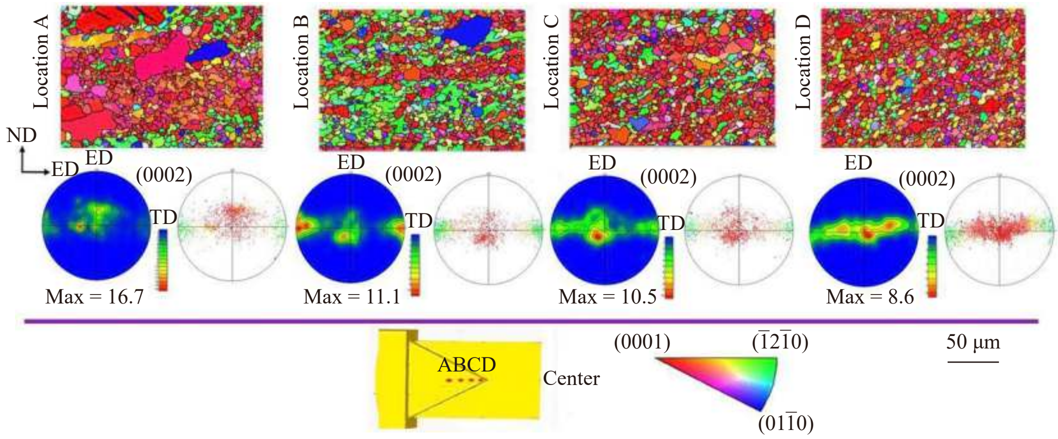

Fig. 3. Microstructure evolutions of workpieces at center region near the extrusion die exit before sheet forming during TGE process.

region is composed of fine and uniform microstructure. The sample at location E shows basal texture characteristic and the texture component along TD decreases in comparison with the sample at location D (Fig. 3), but new texture component along ED appears. At location F, the basal texture component decreases, while the texture component along ED increases. From location G to H, the basal poles incline away from ND to ED. Therefore, the similar texture characteristic is formed in the TGE sheet. The results are consistent with our previous reports [32].

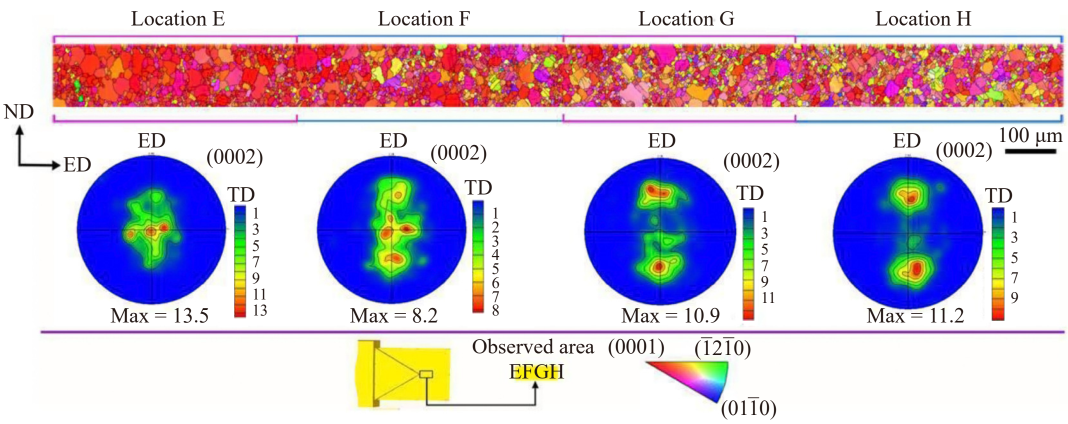

Fig. 4. Microstructure evolutions of workpieces at center region near the extrusion die exit after sheet forming during TGE process.

The microstructure evolutions of workpieces at 1/4 edge region of extruded sheet near the extrusion die exit during TGE process are analyzed, and the results are shown in Fig. 5. Moreover, the microstructure and (0002) pole figures of DRXed grains are also investigated. It can be clearly observed that the microstructures become fine and uniform. Due to the increase of DRXed grains, the maximum intensity of basal poles gradually decreases from 14.7 (location A) to 9.7 (location D). The prismatic orientation grains are gradually replaced by those grains with basal poles parallel to ND because basal slips are activated during extrusion. The corresponding DRXed grains have low basal pole intensity. The basal poles of DRXed grains for the sample at location D are elongated and inclined away from ED to TD, which is similar to the final texture feature of extruded sheet.

3.2. Mechanical properties

Fig. 6 shows true stress (σ)–strain (ε) curves of CE and TGE sheets along ED and TD at room temperature. The yield strength (YS), ultimate strength (UTS), elongation to failure (EI), strain hardening exponent (n-value), and Lankford value (r-value) are summarized in Table 1. The n-value is calculated from $\sigma = K\varepsilon^n$ [34], and the r-value is measured at engineering strain of 8%. The ED-center tensile sample exhibits the lowest YS of 86.5 MPa and the highest EI of 41.0%. However, for the ED-edge tensile sample, the YS increases to 210.3 MPa and the EI decreases to 22.1%. The YS value of ED tensile sample in CE sheet is between those of ED-center and ED-edge tensile samples, but the EI is lower than those of ED-center and ED-edge tensile samples. The TD tensile sample of CE sheet shows the highest YS of 213.2 MPa, but the lowest EI of 18.2%. Meanwhile, the YS for TD sample of TGE sheet decreases to 117.2 MPa, whereas the EI increases to 26.5%. The TGE sheet exhibits higher n-values than the CE sheet, and the n-value reaches the highest value of 0.66 for the ED-center tensile sample. The lower r-values (close to 1) are measured in the ED-center and TD tensile samples for the TGE sheet, compared with those of the CE sheet.

The fracture surface of ED-center tensile sample in the TGE sheet after stretched to failure is investigated, compared with the ED tensile sample in the CE sheet (Fig. 7). The CE

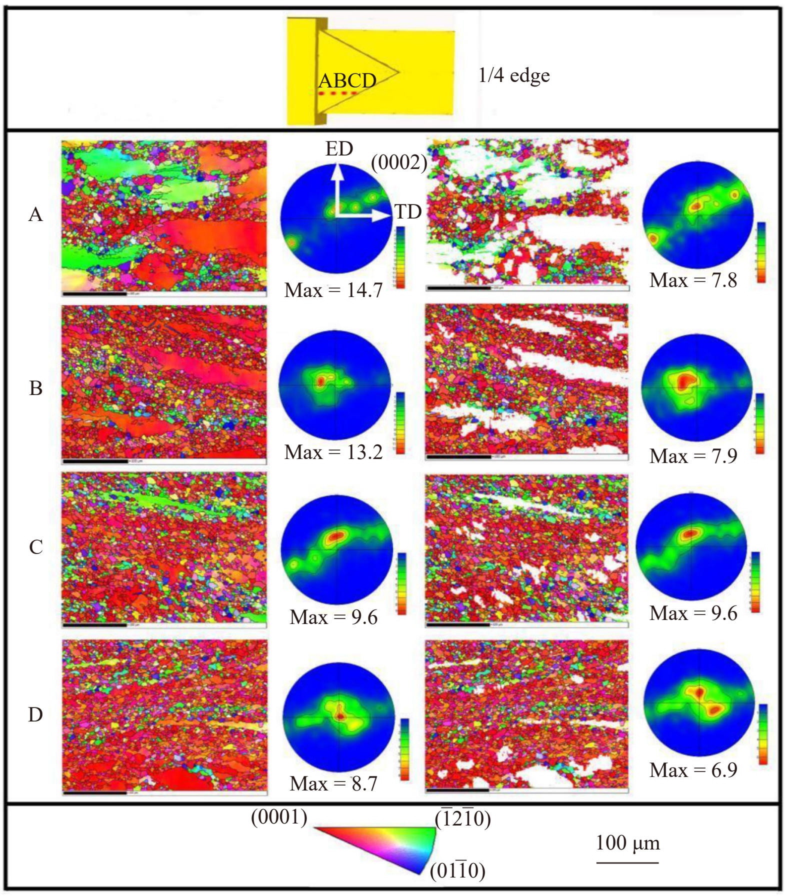

Fig. 5. Microstructure evolutions of workpieces at 1/4 edge region of extruded sheet near the extrusion die exit during TGE process.

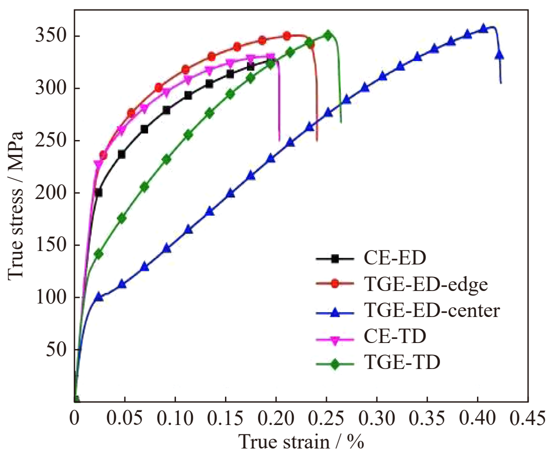

Fig. 6. True stress–strain curves of the CE and TGE sheets.

Table 1. Tensile properties and Lankford values of the CE and TGE sheets at room temperature

Sample		YS / MPa	EI / %	UTS / MPa	n-value	r-value
CE	ED	176.1	18.4	325.9	0.24	1.72
	TD	213.2	18.2	330.5	0.20	3.06
TGE	ED-center	86.5	41.0	357.8	0.66	−0.72
	ED-edge	210.3	22.1	350.1	0.26	2.85
	TD	117.2	26.5	350.7	0.45	1.30

sample exhibits a typical quasi-cleavage characteristic, meaning poor ductility [30]. Large numbers of dimples come out in the ED-center tensile sample, and the volume of cleav-

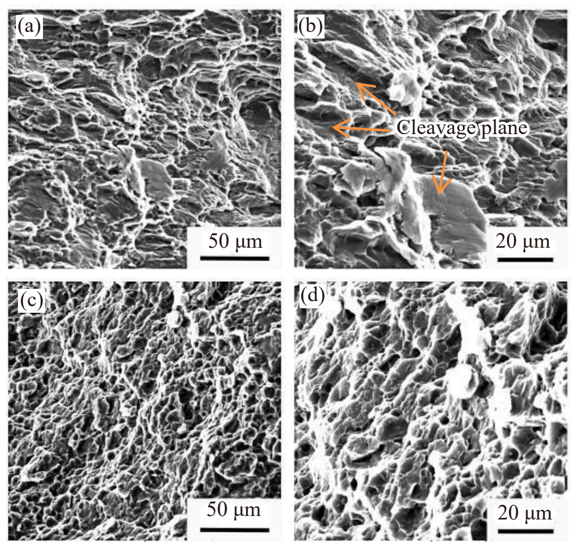

Fig. 7. SEM images of fracture surface obtained from: (a) the CE sample, (b) higher magnification in (a), (c) the TGE sample, and (d) higher magnification in (c).

age surface decreases obviously, indicating the fracture mechanism of extruded sheet during tensile fracture tests changes. Namely, ductile fracture becomes the fracture mode for the ED-center sample [35].

4. Discussion

The TGE process is analyzed by finite element simulation

(FEM). Fig. 8(a) shows the velocity distribution of workpiece near the die outlet obtained from ED–TD plane. The flow velocity direction tilts from ED to TD during extrusion except for center region of extruded sheet, resulting in formation of flow velocities along ED (V_{ED}) and TD (V_{TD}). Thus, the extra velocity along TD (V_{TD}) is formed during TGE process, except for the center region, which might be the reason for the basal poles of TGE sheet tilted away from ED to TD. The velocity evolutions at center (P1), 3/8 edge (P2), 1/4 edge (P3), 1/8 edge (P4), and edge (P5) regions of workpiece along ED (V_{ED}) during TGE process are investigated, as presented in Fig. 8(b). The velocity decreases from the center to edge region of extruded sheet. Thus, an evident velocity gradient is formed along TD. The generation of velocity gradient during extrusion process can form shear stress, leading to the grains with the *c*-axis tilting away from the ND [30]. In addition, the velocity decreases from the center to edge region of extruded sheet during extrusion, which means the velocity gradient relative to the edge region of the alloy decreases. Correspondingly, the basal poles deviation from ND decreases. The basal poles tilt away from ND reaches the maximum ([0002] peak around 65°) for the center region sample and the minimum ([0002] peak around 25°) for the 1/8 edge region sample, respectively.

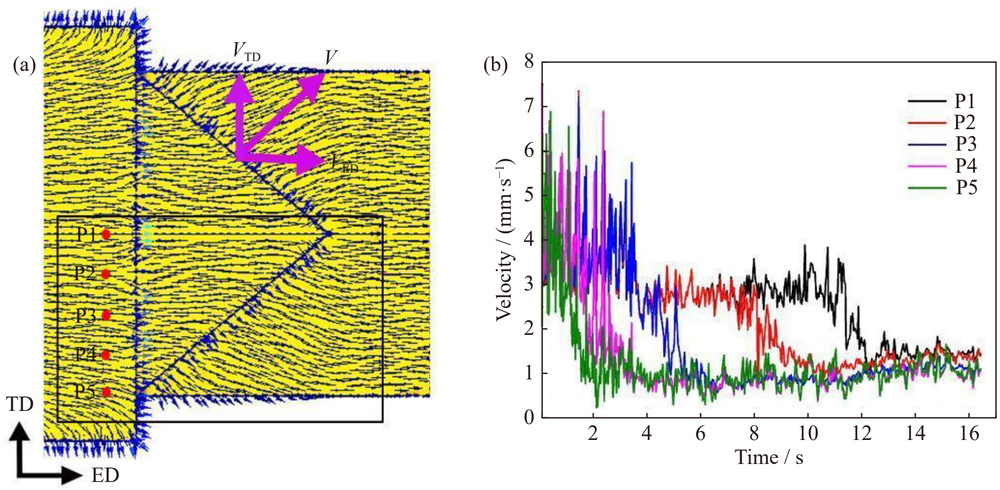

Fig. 8. (a) Flow velocity distribution near the die outlet of workpiece obtained from ED–TD plane, (b) the flow velocity evolutions of P1, P2, P3, P4, and P5 points along ED (V_{ED}) in the black rectangle in (a) during the TGE processes.

The mechanical properties are mainly affected by the microstructures. The CE sheet exhibits a heterogeneous structure and strong basal texture, while TGE sheet has fine uniform microstructure and multi-type unique textures (Fig. 2). Both the ductility and strength of Mg alloys are mainly affected by the grain sizes and textures [36–37].

As described by the standard Hall-Petch relationship, grain refinement can enhance the YS of Mg alloys. Therefore, the YS of ED-edge sample for the TGE sheet with finer microstructure increases compared to that of the CE sheet. However, the YS of ED-center and TD samples for the TGE sheet does not abide by the classical Hall-Petch relationship [38–41]. As the texture modification also plays a significant role in the determination of YS [42]. Since basal <*a*> slip is the main deformation mode for Mg alloys under normal temperature [43–46], the Schmid factors for basal <*a*> slip (SF_{basal}) of the CE, TGE-center, TGE-3/8 edge, TGE-1/4 edge, and TGE-1/8 edge regions samples tensioned along the ED and TD are shown in Fig. 9. When tensioned along ED, the SF_{basal} of CE sample is lower than those of the TGE-center and TGE-3/8 edge regions samples, but higher than those of TGE-1/4 and TGE-1/8 edge region samples. The SF_{basal} increases gradually from edge to center region of the TGE sheet, which means that the basal <*a*> slip for the ED-center tensile sample is easily to be activated. Hence, the ED-center tensile sample exhibits a lower YS than ED-edge and CE tensile samples. Obviously, the average SF_{basal} for the TGE sheet tensioned along TD are higher than that of the CE sheet, especially for the TGE-3/8 edge region sample. The higher SF_{basal} of the TGE sheet leads to lower YS than the CE sheet when tensioned along the TD.

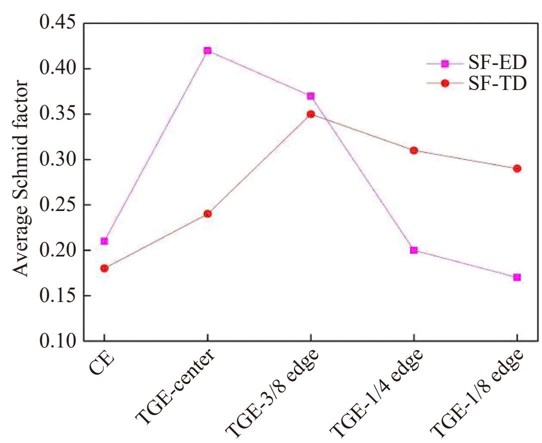

Fig. 9. Average Schmid factors for basal slip of CE, TGE-center, TGE-3/8 edge, TGE-1/4 edge, and TGE-1/8 edge regions samples.

The TGE sheet exhibits higher EI than CE sheet, which is associated with grain sizes and textures. The grain refinement can effectively enhance grain boundaries collaborating ability during deformation [47]. Macro-deformation is accompanied by micro-dislocation movement because of the basal <*a*> slip activity. A great number of dislocations are formed and interact with each other, resulting in the enhancement of local strain hardening behavior [48]. Thus, the EI is ameliorated. The TGE sheet has basal poles leaned away from the ND, which is good for the basal <*a*> slip activity. Consequently, the TGE sheet exhibits low *r*-value and high *n*-value [49].

The ED-center tensile sample for the TGE sheet exhibits the lowest YS of 86.5 MPa and the highest EI of 41.0%. In order to better understand the reason, the microstructure and texture evolutions after tensile deformation to a strain of 8% are investigated and compared with ED sample for the CE sheet, as shown in Fig. 10. Compared with the un-stretched CE sample (Fig. 2), the angular distribution of the basal poles becomes narrow toward to ND and the maximum pole intensity increases (Fig. 10(a)). However, the maximum pole intensity decreases and the distribution of basal poles becomes scattered for the TGE sample. In addition, more $\{10\bar{1}2\}$ tension twins are observed in the TGE samples than CE one, which implies that the tensile twins are more easily activated during deformation. Intragranular misorientation axis (IGMA) analysis is an effective method to distinguish the dislocation slip type of hcp metals. The grains within a misorientation of 1°–3° are used for analysis. The pyramidal dislocation slips with the highest critical resolved shear stress (CRSS) can be hardly activated in AZ31 alloy at room temperature [50–51]. Thus, non-basal dislocation is considered as a prismatic dislocation. For CE sheet, the misorientation axis tends to have a concentration close to <0001>, indicating the prismatic <*a*> slip is the dominant deformation mechanism [52]. In the case of TGE sheet, the <*uvt*0> distribution is associated with the activation of basal <*a*> slip.

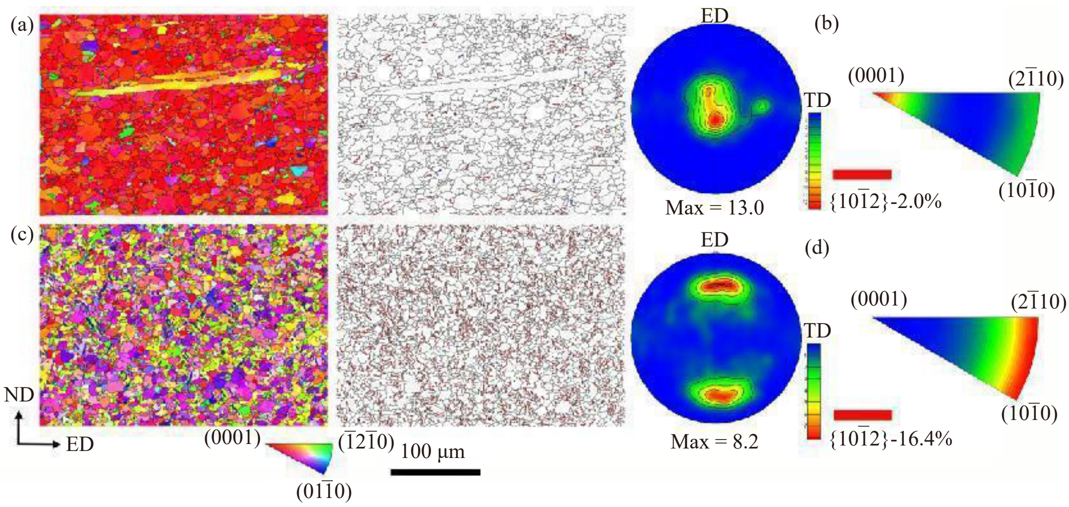

Fig. 10. (a, c) EBSD IPF maps and (b, d) IGMA distribution of various tensile samples at a strain of 8%: (a, b) ED sample in the CE sheet; (c, d) ED-center sample in the TGE sheet.

5. Conclusions

In this work, we researched the effect of TGE and CE processes on the microstructures, textures, and mechanical properties of AZ31 sheet. The flow behavior and dynamic recrystallization during TGE process were investigated. The conclusions are summarized as follows:

(1) The extra flow velocity along TD and velocity gradient along ED could be effectively introduced during TGE process, which resulted in fine grain size and multi-type unique textures obtained in TGE sheet. From edge to center of the TGE sheet, the basal poles gradually deviated from the ND. The largest inclination for the sample at center region reached around 65°. Furthermore, the basal poles inclined from ED to TD 40°–63°, except for the center region of TGE sheet.

(2) Compared with CE sheet, the TGE sheet with fine grain microstructure and multi-type unique textures showed higher ductility and *n*-value, but lower yield strength and *r*-value. As the tension twins and basal <*a*> slip are easy to be activated during deformation, the largest elongation of 41% and the lowest yield strength of 86.5 MPa were obtained in the ED-center sample for the TGE sheet.

Acknowledgements

This work was financially supported by the Guangdong Academy of Science Fund (No. 2020GDASYL-2020 0101001), the Guangdong Major Project of Basic and Applied Basic Research (No. 2020B0301030006), the China Postdoctoral Science Foundation (No. 2022M720858), the Scientific Research Fund of Hunan Provincial Education Department (No. 21B0726), the National Natural Science Foundation of China (Nos. U1764253, 51971044, U191 0213, 52001037, and U207601), the Qinghai Scientific & Technological Program (No. 2018-GX-A1), and the Natural Science Foundation of Chongqing, China (No. cstc2019jcyj-msxmX0234). The authors also thank Mrs. Mingmin Li for proofreading the manuscript.

Conflict of Interest

The authors declare no conflict of interest.

References

[1] N. Li, C. Wang, M.A. Monclús, L. Yang, and J.M. Molina-Aldareguia, Solid solution and precipitation strengthening effects in basal slip, extension twinning and pyramidal slip in Mg–Zn alloys, *Acta Mater.*, 221(2021), art. No. 117374.

[2] F.Y. Liu, R.L. Xin, M.X. Zhang, M.T. Pérez-Prado, and Q. Liu, Evaluating the orientation relationship of prismatic precipitates generated by detwinning in Mg alloys, *Acta Mater.*, 195(2020), p. 263.

[3] J.Q. Hao, J.S. Zhang, H.X. Wang, W.L. Cheng, and Y. Bai, Microstructure and mechanical properties of Mg–Zn–Y–Mn magnesium alloys with different Zn/Y atomic ratio, *J. Mater. Res. Technol.*, 19(2022), p. 1650.

[4] A.V. Koltygin, V.E. Bazhenov, I.V. Plisetskaya, *et al.*, Influence of Zr and Mn additions on microstructure and properties of Mg–2.5wt%Cu–*X*wt%Zn (X = 2.5, 5 and 6.5) alloys, *Int. J. Miner. Metall. Mater.*, 29(2022), No. 9, p. 1733.

[5] M.Z. Bian, X.S. Huang, and Y. Chino, Substantial improvement in cold formability of concentrated Mg–Al–Zn–Ca alloy sheets by high temperature final rolling, *Acta Mater.*, 220(2021), art. No. 117328.

[6] J. Zheng, Z. Chen, Z.M. Yan, Z.M. Zhang, Q. Wang, and Y. Xue, Preparation of ultra-high strength Mg–Gd–Y–Zn–Zr alloy by pre-ageing treatment prior to extrusion, *J. Alloys Compd.*, 894(2022), art. No. 162490.

[7] H. Pang, J. Bao, Q.A. Li, *et al.*, Effect of Sm on microstructures and mechanical properties of Mg–Gd(–Sm)–Zr alloys by hot extrusion and aging treatment, *J. Mater. Res. Technol.*, 19(2022), p. 3877.

[8] Z.K. Deng, X.P. Li, S.Z. Wang, X.H. Li, D.X. Chen, and X.F. Xiao, Texture tailoring of a cold-rolled Mg–Zn–Gd alloy by electropulse treatment: The effect of electropulse and Gd element, *Mater. Charact.*, 190(2022), art. No. 112046.

[9] Z. Zhang, J.H. Zhang, J. Wang, *et al.*, Toward the development of Mg alloys with simultaneously improved strength and ductility by refining grain size via the deformation process, *Int. J. Miner. Metall. Mater.*, 28(2021), No. 1, p. 30.

[10] T. Tsuru, H. Somekawa, and D.C. Chrzan, Interfacial segregation and fracture in Mg-based binary alloys: Experimental and first-principles perspective, *Acta Mater.*, 151(2018), p. 78.

[11] J. Koike, T. Kobayashi, T. Mukai, *et al.*, The activity of non-basal slip systems and dynamic recovery at room temperature in fine-grained AZ31B magnesium alloys, *Acta Mater.*, 51(2003), No. 7, p. 2055.

[12] J. Zhao, B. Jiang, Y. Song, *et al.*, Simultaneous improvement of strength and ductility by Mn addition in extruded Mg–Gd–Zn alloy, *Trans. Nonferrous Met. Soc. China*, 32(2022), No. 5, p. 1460.

[13] Y. Wang and H. Choo, Influence of texture on Hall-Petch relationships in an Mg alloy, *Acta Mater.*, 81(2014), p. 83.

[14] S. Basu, E. Dogan, B. Kondori, I. Karaman, and A.A. Benzerga, Towards designing anisotropy for ductility enhancement: A theory-driven investigation in Mg-alloys, *Acta Mater.*, 131(2017), p. 349.

[15] D.D. Zhang, C.M. Liu, S.N. Jiang, Y.C. Wan, and Z.Y. Chen, Effects of trace Ag on precipitation behavior and mechanical properties of extruded Mg–Gd–Y–Zr alloys, *Trans. Nonferrous Met. Soc. China*, 31(2021), No. 11, p. 3394.

[16] Y.J. Ma, C.M. Liu, S.N. Jiang, Y.C. Wan, and Z.Y. Chen, Microstructure, mechanical properties and damping capacity of as-extruded Mg–1.5Gd alloys containing rare-earth textures, *Mater. Charact.*, 189(2022), art. No. 111969.

[17] K.B. Nie, X.J. Wang, K.K. Deng, F.J. Xu, K. Wu, and M.Y. Zheng, Microstructures and mechanical properties of AZ91 magnesium alloy processed by multidirectional forging under decreasing temperature conditions, *J. Alloys Compd.*, 617(2014), p. 979.

[18] M. Pérez-Prado, J.A. del Valle, and O.A. Ruano, Achieving high strength in commercial Mg cast alloys through large strain rolling, *Mater. Lett.*, 59(2005), No. 26, p. 3299.

[19] X. Che, B.B. Dong, Q. Wang, *et al.*, The effect of processing parameters on the microstructure and texture evolution of a cup-shaped AZ80 Mg alloy sample manufactured by the rotating backward extrusion, *J. Alloys Compd.*, 854(2021), art. No. 156264.

[20] J.W. Kang, X.F. Sun, K.K. Deng, F.J. Xu, X. Zhang, and Y. Bai, High strength Mg–9Al serial alloy processed by slow extrusion, *Mater. Sci. Eng. A*, 697(2017), p. 211.

[21] J. Xu, B. Jiang, Y.H. Kang, *et al.*, Tailoring microstructure and texture of Mg–3Al–1Zn alloy sheets through curve extrusion process for achieving low planar anisotropy, *J. Mater. Sci. Technol.*, 113(2022), p. 48.

[22] H. Jafari, A.H.M. Tehrani, and M. Heydari, Effect of extrusion process on microstructure and mechanical and corrosion properties of biodegradable Mg–5Zn–1.5Y magnesium alloy, *Int. J. Miner. Metall. Mater.*, 29(2022), No. 3, p. 490.

[23] X. Zhao, S.C. Li, Y.S. Zheng, *et al.*, The microstructure evolution, texture weakening mechanism and mechanical properties of AZ80 Mg alloy processed by repetitive upsetting-extrusion with reduced deformation temperature, *J. Alloys Compd.*, 883(2021), art. No. 160871.

[24] X. Li, C. Liu, J.S. Wang, and C. Zhang, Tailoring the strength and formability of Mg alloys through rare earth element additions (Gd and Dy) and dynamic recrystallizations, *Mater. Today Commun.*, 28(2021), art. No. 102627.

[25] A. Imandoust, C.D. Barrett, T. Al-Samman, K.A. Inal, and H.E. Kadiri, A review on the effect of rare-earth elements on texture evolution during processing of magnesium alloys, *J. Mater. Sci.*, 52(2017), No. 1, p. 1.

[26] G. Zhou, Y. Yang, L. Sun, *et al.*, Tailoring the microstructure, mechanical properties and damping capacities of Mg–4Li–3Al–0.3Mn alloy via hot extrusion, *J. Mater. Res. Technol.*, 19(2022), p. 4197.

[27] W.X. Fan, Y. Bai, G.Y. Li, X.Y. Chang, and H. Hao, Enhanced mechanical properties and formability of hot-rolled Mg–Zn–Mn alloy by Ca and Sm alloying, *Trans. Nonferrous Met. Soc. China*, 32(2022), No. 4, p. 1119.

[28] T. Nakata, C. Xu, and S. Kamado, Formation of anomalous twinning and its effect on texture development in a cold-rolled Mg–Zn–Ca alloy sheet, *Mater. Charact.*, 181(2021), art. No. 111507.

[29] J. Zhao, B. Jiang, Q.H. Wang, *et al.*, Effects of Li addition on the microstructure and tensile properties of the extruded Mg–1Zn–*x*Li alloy, *Int. J. Miner. Metall. Mater.*, 29(2022), No. 7, p. 1380.

[30] J. Xu, J.F. Song, B. Jiang, *et al.*, Effect of effective strain gradient on texture and mechanical properties of Mg–3Al–1Zn alloy sheets produced by asymmetric extrusion, *Mater. Sci. Eng. A*, 706(2017), p. 172.

[31] Q.H. Wang, J.F. Song, B. Jiang, *et al.*, An investigation on microstructure, texture and formability of AZ31 sheet processed by asymmetric porthole die extrusion, *Mater. Sci. Eng. A*, 720(2018), p. 85.

[32] J. Xu, W.J. Liu, B. Jiang, *et al.*, Forming novel texture and enhancing the formability in Mg–3Al–Zn alloy sheets fabricated by transverse gradient extrusion, *J. Mater. Res. Technol.*, 18(2022), p. 3143.

[33] Z.J. Yu, C. Xu, J. Meng, X.H. Zhang, and S. Kamado, Microstructure evolution and mechanical properties of as-extruded Mg–Gd–Y–Zr alloy with Zn and Nd additions, *Mater. Sci. Eng. A*, 713(2018), p. 234.

[34] C.Y. Zhao, X.H. Chen, F.S. Pan, S.Y. Gao, D. Zhao, and X.F. Liu, Effect of Sn content on strain hardening behavior of as-extruded Mg–Sn alloys, *Mater. Sci. Eng. A*, 713(2018), p. 244.

[35] Q. Kang, H.T. Jiang, Y. Zhang, Z. Xu, H. Li, and Z.H. Xia, Effect of various Ca content on microstructure and fracture toughness of extruded Mg–2Zn alloys, *J. Alloys Compd.*, 742(2018), p. 1019.

[36] Y. Liu, J.B. Wen, H. Li, and J.G. He, Effects of extrusion parameters on the microstructure, corrosion resistance, and mechanical properties of biodegradable Mg–Zn–Gd–Y–Zr alloy, *J. Alloys Compd.*, 891(2022), art. No. 161964.

[37] L. Yan, Z.M. Zhang, Y. Xue, J. Xu, B.B. Dong, and X.B. Li, Effect of rotating shear extrusion on the microstructure, texture evolution and mechanical properties of Mg–Gd–Y–Zn–Zr alloy, *J. Alloys Compd.*, 906(2022), art. No. 164406.

[38] P. Minárik, R. Král, J. Čížek, and F. Chmelík, Effect of different *c*/*a* ratio on the microstructure and mechanical properties in magnesium alloys processed by ECAP, *Acta Mater.*, 107(2016), p. 83.

[39] J. Hofstetter, S. Rüedi, I. Baumgartner, *et al*., Processing and microstructure–property relations of high-strength low-alloy (HSLA) Mg–Zn–Ca alloys, *Acta Mater.*, 98(2015), p. 423.

[40] K. Guan, R. Ma, J.H. Zhang, R.Z. Wu, Q. Yang, and J. Meng, Modifying microstructures and tensile properties of Mg–Sm based alloy via extrusion ratio, *J. Magnes. Alloys*, 9(2021), No. 3, p. 1098.

[41] X.Z. Jin, W.C. Xu, D.B. Shan, B. Guo, and B.C. Jin, Mechanism of high-strength and ductility of Mg–RE alloy fabricated by low-temperature extrusion and aging treatment, *Mater. Des.*, 199(2021), art. No. 109384.

[42] S.R. Agnew, J.A. Horton, T.M. Lillo, and D.W. Brown, Enhanced ductility in strongly textured magnesium produced by equal channel angular processing, *Scripta Mater.*, 50(2004), No. 3, p. 377.

[43] C. He, S.W. Bai, B. Jiang, *et al*., Effect of Gd content on the microstructure, texture and mechanical properties of Mg–*x*Gd–0.5Mn alloys, *J. Mater. Res. Technol.*, 20(2022), p. 343.

[44] Z.C. Li, J.M. Yu, D.L. Lu, *et al*., Synergistic effects of grain refinement and texture weakening on mechanical properties anisotropy of Mg–9Gd–4Y–2Zn–0.4Zr alloy via RUE processing, *J. Mater. Res. Technol.*, 19(2022), p. 837.

[45] J.S. Wei, C.M. Liu, Y.C. Wan, J.B. Shao, X.Z. Han, and G.L. Zhang, Strengthening against $\{10\bar{1}2\}$ twinning by discontinuous and continuous precipitate in a strongly textured Mg–9Al alloy, *Mater. Charact.*, 167(2020), art. No. 110523.

[46] H.B. Yang, Y.F. Chai, B. Jiang, *et al*., Enhanced mechanical properties of Mg–3Al–1Zn alloy sheets through slope extrusion, *Int. J. Miner. Metall. Mater.*, 29(2022), No. 7, p. 1343.

[47] Q.H. Wang, Y.Q. Shen, B. Jiang, *et al*., A good balance between ductility and stretch formability of dilute Mg–Sn–Y sheet at room temperature, *Mater. Sci. Eng. A*, 736(2018), p. 404.

[48] L. Zhang, G.S. Huang, H. Zhang, and B. Song, Cold stamping formability of AZ31B magnesium alloy sheet undergoing repeated unidirectional bending process, *J. Mater. Process. Technol.*, 211(2011), No. 4, p. 644.

[49] J.R. Dong, D.F. Zhang, J. Sun, Q.W. Dai, and F.S. Pan, Effects of different stretching routes on microstructure and mechanical properties of AZ31B magnesium alloy sheets, *J. Mater. Sci. Technol.*, 31(2015), No. 9, p. 935.

[50] M. Sanjari, A. Farzadfar, A.S.H. Kabir, *et al*., Promotion of texture weakening in magnesium by alloying and thermomechanical processing: (I) alloying, *J. Mater. Sci.*, 49(2014), No. 3, p. 1408.

[51] C. Ha, J. Bohlen, X. Zhou, *et al*., Texture development and dislocation activities in Mg–Nd and Mg–Ca alloy sheets, *Mater. Charact.*, 175(2021), art. No. 111044.

[52] Y.B. Chun and C.H.J. Davies, Investigation of prism <*a*> slip in warm-rolled AZ31 alloy, *Metall. Mater. Trans. A*, 42(2011), No. 13, p. 4113.